P. 33

"Gamma Ray Astronomy"

FINAL REPORT

Contract NAS8-36955
Delivery Order Number 42

July 13, 1989 - January 12, 1991

Prepared by

Dr. William S. Paciesas

Prepared for
George C. Marshall Space Flight Center
National Aeronautics and Space Administration
Marshall Space Flight Center, Alabama 35812

Submitted by
Department of Physics
The University of Alabama in Huntsville
Huntsville, Alabama 35899

January 1991

W. Paciesas served as BATSE Mission Operations (MOPS) Software Development Manager and also chaired the Level V Configuration Control Board for the MOPS software. The MOPS Software Test Readiness Review (TRR) was held on September 13, 1989, and the MOPS Software Functional Configuration Inspection (FCI) was held on May 8, 1990. Paciesas organized the TRR and FCI and also presented the status of MOPS software development at the GRO Project Software Review on January 23, 1990, and at BATSE Science Team Meetings in November, 1989, and June and November, 1990. Various builds of the software were used to support GRO end-to-end tests in October and November, 1989, and March, June, July, August, and November, 1990. Data from end-to-end tests, most notably ETE #4 and #7, were used extensively for beta testing of the MOPS software. During the period of performance of this delivery order the following units completed unit testing and were placed under configuration control: SEND_MESSAGE, SENDER, INST_MODEL_EDITOR, INST_CONFIG_MONITOR, X25_MANAGER, SOURCE_CATALOG_EDITOR, CHECK_CPU_MEMORY, GET_DATA, GET_TIME, SET_QUALITY_FLAGS, ADD_QUALITY_FLAGS, MESSAGE_HANDLER, SPECIFY_QUALITY_MASK, PACKET_DATA_HANDLER, ORBIT_HISTORY_EDITOR, DET_EFFICIENCY, COMMAND_FILE_GENERATOR, BURST_LOCATION and OCCULTATION_SEARCH. Of the ten remaining units, coding is nominally complete on all but one. However, the consensus of the BATSE science team was that beta testing by the potential users prior to initial configuration control was warranted and is currently in progress.

P. Moore provided administrative assistance in the MOPS software development effort and was also given the responsibility to code and test the BURST_DISPLAY unit. Moore developed procedures for converting System Test Software (STS) data tapes into MOPS daily datasets and organizing the resulting database. Moore attended a training course "INGRES for Application Developers SQL" in March, 1990, and has been advising other BATSE programmers on INGRES as required.

Paciesas continued to serve as the BATSE representative on the GRO Data Operations Group (GRODOG) and the GRO Users' Committee, attending meetings in July and November, 1989, and January, March, May and October, 1990. In this regard he provided BATSE inputs for the NASA Research Announcement for the GRO Guest Investigator program [1] which was issued in January, 1990, and the GRO Project Data Management Plan [2] which was released in July, 1990, and the proposal for the GRO Fellowship Program, the announcement for which is expected to be issued in January, 1991.

Beginning in April, 1990, Paciesas was named as BATSE representative on the calibration review teams for the other GRO instruments. In this capacity, he attended Calibration Reviews for EGRET at GSFC and OSSE at NRL, both in May, 1990, and for COMPTEL at MPI Garching in July, 1990, and co-authored review reports for each of these.

Paciesas also served as scientific liaison overseeing development of the BATSE Spectral Analysis Software (BSAS) by GSFC. G. Pendleton assisted in scientific validation of the model-independent spectral deconvolution algorithm developed for BSAS by B. Schaefer (GSFC). Pendleton and K. Hong analyzed data from balloon flights of BATSE-type detectors and showed that the known spectrum of the Crab Nebula could be satisfactorily reproduced using Schaefer's technique (Figure 1). The progress of BSAS software development was reviewed at the BATSE Science Team Meetings in November, 1989, June, 1990, and November, 1990, and at the GRO Project Software Review in January, 1990. The first build of the software completed testing in February and was received by MSFC for installation in early March. The build included the modules REDUCE, MODFIT, QFIT, QPHOTN, PHOTON, and MATRIX, plus INGRES tables and some additional utilities for generating test data. A second build, including the modules COUNT and SPPLOT, plus updated versions of MATRIX, MODFIT, QFIT and QPHOTN, is to be delivered to MSFC and UCSD in December, 1990.

Paciesas coordinated efforts by UCSD to participate in BATSE data analysis. The extensive UCSD experience with modeling detector backgrounds on the HEAO A-4 instrument provided a natural starting point for modeling BATSE detector backgrounds. Paciesas visited UCSD in March, 1990, to formulate plans for UCSD participation and later met with UCSD scientists in conjunction with the BATSE Science Team Meetings in June and November, 1990. In November, UCSD provided copies of a number of software routines which were developed for analysis of HEAO A-4 detector background. A. Harmon (USRA) is currently investigating conversion of these for use by BATSE.

G. Pendleton has led the joint UAH/MSFC effort to develop detector response matrices suitable for use with the BSAS spectral deconvolution algorithms. In this context, he collaborated with P. Lestrade (Miss. St. U.) on quantifying channel-to-energy conversion algorithms for BATSE detectors. He presented status reports on these issues at the GRO Project Software Review in January, 1990, at the BATSE Calibration Review in June, 1990, and at BATSE Science Team Meetings in June, 1990, and November, 1990. Paciesas presented some early calibration results at the SPIE Workshop on EUV, X-Ray, and Gamma-Ray Instrumentation for Astronomy and Atomic Physics in August, 1989 [3, attached as Appendix A]. Working with E. Roberts (MSFC), Pendleton produced an interim report for circulation to the BATSE science team on simulations of atmospheric scattering [4, attached as Appendix B].

Pendleton served as BATSE representative to the GRO Mass Model Committee, attending meetings in January, April, and November, 1990. In an effort to keep abreast of current developments in Monte Carlo simulation of gamma-ray and particle interactions, he attended the CALOR 89 conference in September, 1989.

Pendleton and Paciesas, in collaboration with MSFC scientists, used a deconvolution methodology similar to that of BSAS to produce deconvolved spectra from balloon-borne observations of supernova 1897A. For this purpose Pendleton produced detector response matrices using the same Monte Carlo techniques developed for BATSE. Results were presented at the American Astronomical Society meeting in Washington, DC, in January, 1990 [5, attached as Appendix C]. Figure 2 is a summary of these results, comparing the deconvolved experimental data with theoretical simulations.

Pendleton, Moore and Flickinger provided remote operations support during various BATSE test activities: Pendleton supported instrument data runs at TRW in October, 1989 and he assisted in monitoring instrument subsystems at KSC during ETE's #4, #6, and #7. Pendleton and Flickinger assisted in instrument activation simulation operations at GSFC during ETE #5 and Moore assisted in monitoring instrument subsystems at KSC during this same test. Flickinger represented BATSE at the GRO Test Review Board meeting at KSC in April, 1990.

Under subcontract to UAH, Teledyne-Brown Engineering (TBE) developed software for use in predicting encounters between GRO and Earth-orbiting spacecraft that are suspected of carrying operational nuclear reactors. The Gamma Ray Observatory Support System (GROSS) is a custom modification of the SATRAK software system for IBM compatible PC's which TBE developed and maintains for AFSPACECOM. The package permits maintenance of a list of candidate spacecraft and their orbital elements, calculates times that GRO is in line of sight with a candidate spacecraft, and calculates the distance between GRO and the candidate spacecraft as a function of time. Various combinations of data plots may be displayed on the screen and/or sent to a hardcopy device. The software was delivered to MSFC and a training/orientation session conducted on April 2, 1990 by TBE personnel. Five sets of documentation were provided, consisting of the GROSS Operator's Guide [6] and the GROSS Validation Runs [7].

REFERENCES

[1] *Gamma Ray Observatory (GRO) Phase 1 Guest Investigator Program*, NASA Research Announcement 90-OSSA-4, January 30, 1990.

[2] *Gamma Ray Observatory Project Data Management Plan*, NASA unnumbered, July, 1990.

[3] Paciesas, W. S., Pendleton, G. N., Lestrade, J. P., Fishman, G. J., Meegan, C. A., Wilson, R. B., Parnell, T. A., Austin, R. W., Berry, F. A., Jr., Horack, J. M., and Storey, S. D. "Performance of the large-area detectors for the Burst and Transient Source Experiment (BATSE) on the Gamma Ray Observatory." *EUV, X-Ray, and Gamma-Ray Instrumentation for Astronomy and Atomic Physics*, Charles J. Hailey. Oswald H. W. Siegmund, Editors, Proc. SPIE 1159, 156 (1989).

[4] Pendleton, G. N., and Roberts, F. E. "Some Results from Atmospheric Scattering Simulations." UAH preprint (1990).

[5] Pendleton, G. N., Paciesas, W. S., Wilson, R. B., Fishman, G. J., and Meegan, C. A. "Hard X-Ray Continuum Spectra of SN1987A." *Bull. AAS*, **21**, 1214 (1989).

[6] *Gamma Ray Observatory Support System Operator's Guide, Version 1*, TBE Technical Report CS90-UAH-001, March, 1990.

[7] *Gamma Ray Observatory Support System Validation Runs*, TBE Technical Report CS90-UAH-002, March, 1990.
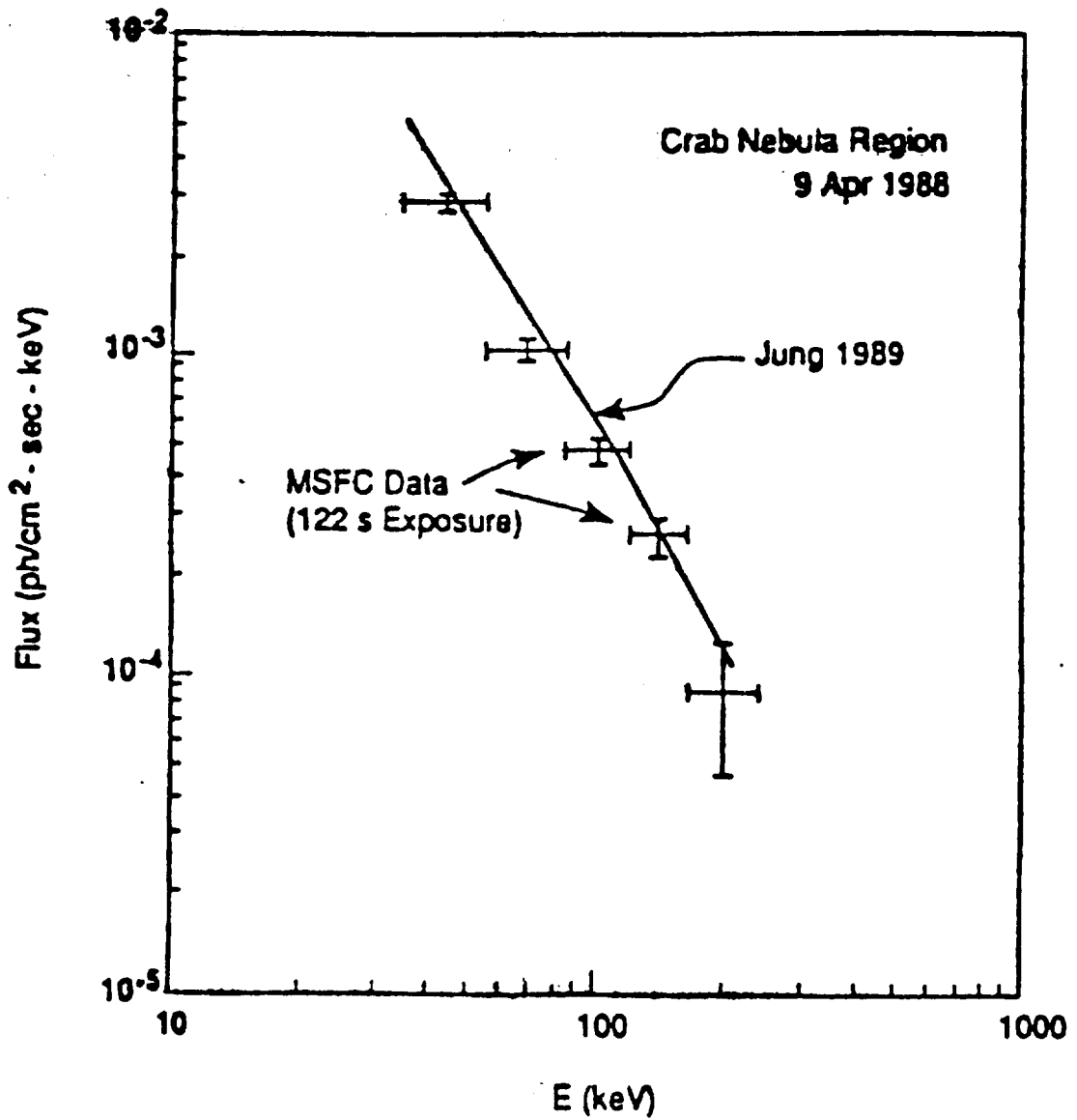
Figure 1. Hard x-ray spectrum of the Crab Nebula obtained with a
112 second observation on the balloon flight of April 9, 1988.
The data have been deconvolved using a model-independent
inversion algorithm. Shown for comparison is the spectrum
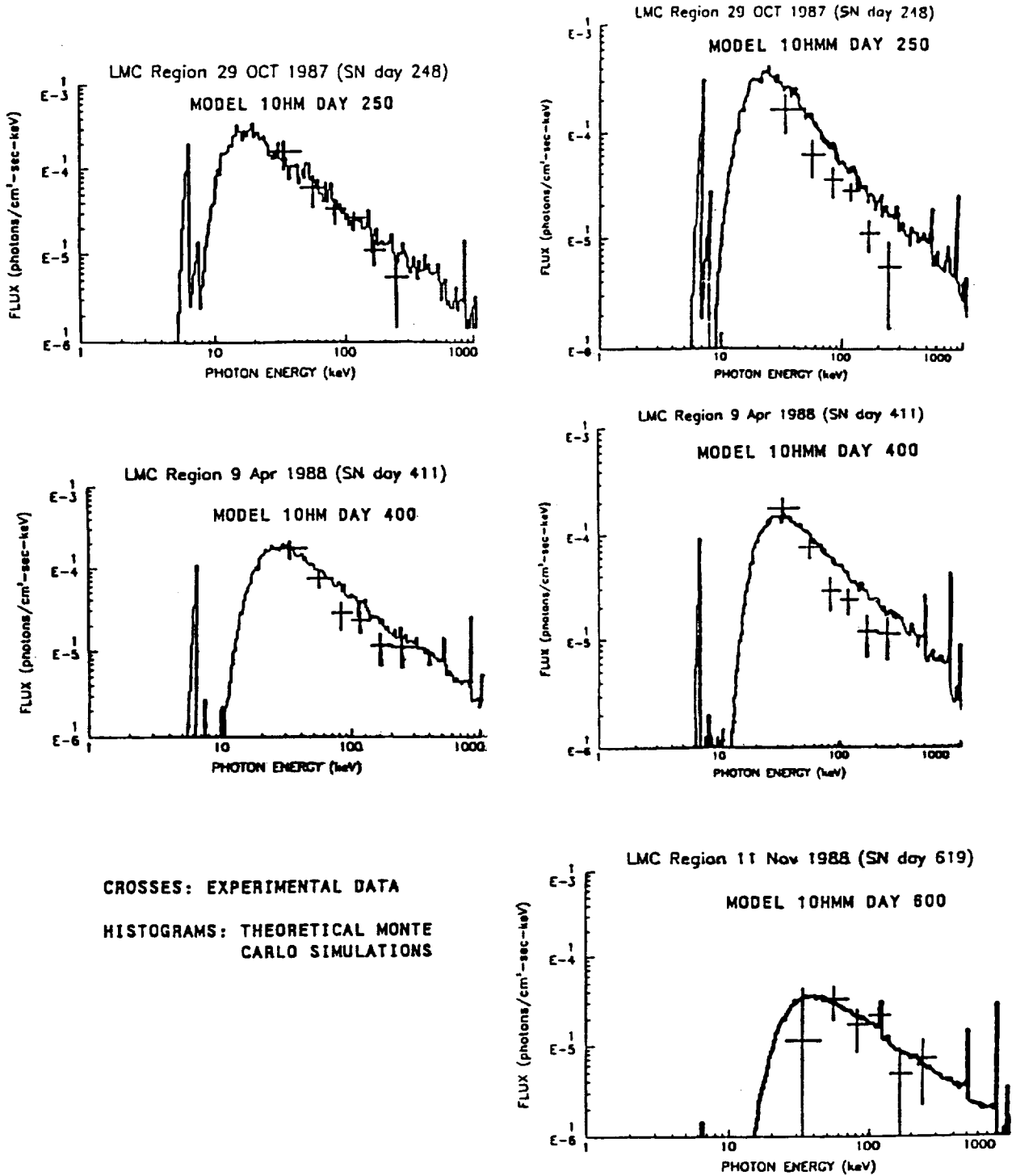obtained by Jung (*Ap. J.*, **338**, 972, 1989).

Figure 2. Deconvolved hard x-ray spectra of supernova 1987A obtained during balloon flights of collimated versions of the BATSE large-area detectors in 1987 and 1988. The experimental data are shown as crosses. The histograms are the results of theoretical Monte Carlo simulations using two different supernova models (Pinto and Woosley, *Nature*, **333**, 534, 1988; Pinto and Woosley, *Ap. J.*, **329**, 820, 1988; Woosley, Pinto, and Hartmann, *Ap. J.*, **346**, 395, 1989).

Appendix A

(Published in SPIE Proceedings, Volume 1159, 1989)

Performance of the large-area detectors
for the Burst and Transient Source Experiment (BATSE)
on the Gamma Ray Observatory

W. S. Paciesas and G. N. Pendleton

Department of Physics and Center for Space Plasma and Aeronomic Research
University of Alabama in Huntsville, AL 35899

J. P. Lestrade

Department of Physics and Astronomy
Mississippi State University, Mississippi State, MS 39762

G. J. Fishman, C. A. Meegan, R. B. Wilson, T. A. Parnell,
R. W. Austin, F. A. Berry, Jr., J. M. Horack and S. D. Storey

Space Science Laboratory
NASA/Marshall Space Flight Center, Huntsville, AL 35812

ABSTRACT

The Burst and Transient Source Experiment (BATSE), one of four experiments on the Gamma Ray Observatory (GRO), is expected to provide the most sensitive observations of γ-ray bursts yet obtained, as well as to provide long-term monitoring of hard x-ray and low-energy γ-ray emission from bright pulsating sources, transients, and solar flares. Eight uncollimated modules, positioned at the corners of the spacecraft to provide an unobstructed view of the sky, detect sources by various techniques based on time variability. Use of detectors with anisotropic response allows location of γ-ray bursts to be determined to an accuracy of $\sim 1°$ using BATSE data alone. The completed BATSE underwent intensive testing and calibration prior to its delivery in October 1988 for integration on the GRO. We describe the instrument and summarize the results of the testing and calibration as they relate to characterization of systematic uncertainties in BATSE burst location.

1. INTRODUCTION

A principal difficulty in understanding the nature of γ-ray bursts is that the distance to them is not known. Identification of the bursts with known objects could provide this information, but attempts to do so have generally been unsuccessful. The situation is further complicated by the fact that distinct classes of bursts may have different properties and physically different origins. BATSE will detect and localize hundreds of γ-ray bursts per year. Such a large sample will be required in order to infer the spatial distribution of the various classes, providing in turn the possibility of associating the bursts with other astrophysical objects. BATSE also has unprecedented sensitivity for performing spectroscopy and studies of rapid variability in bursts.

We describe herein some of the testing, calibration, and simulation that are required in order to assure that BATSE meets its design goals. Specifically, we consider the problem of burst location and its associated uncertainty.

2. INSTRUMENT DESCRIPTION

BATSE has been described in detail elsewhere.[1] It consists of eight uncollimated detector modules placed at the corners of the GRO to provide the maximum unobstructed view of the celestial sphere. Each module includes two NaI(Tℓ) scintillation detectors: a relatively thin large-area detector (LAD) optimized for sensitivity and directional response, and a relatively thick smaller-area spectroscopy detector (SD) optimized for energy resolution and wider
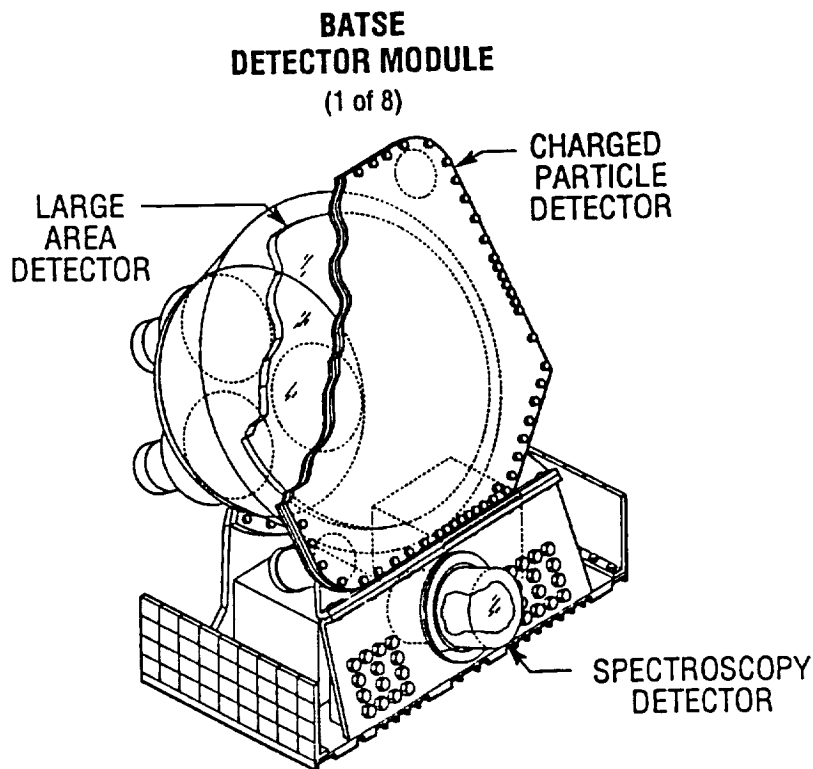
Figure 1: Pictorial representation of a BATSE module.

energy coverage. The anisotropic directional response of the LADs allows location of γ-ray bursts to be determined using BATSE data alone.

The eight planes of the LADs are parallel to the eight faces of a regular octahedron, thus providing nearly uniform sky coverage. The three primary axes of the octahedron are parallel to the three principal axes of the spacecraft. Since the faces of a regular octahedron comprise four intersecting sets of mutually parallel planes, every burst will be viewed by four detectors.

A BATSE module is shown schematically in Figure 1. The LAD contains a NaI(Tℓ) crystal 50.8 cm in diameter and 1.27 cm thick. At low energies where the crystal is opaque to incident radiation, the large diameter-to-thickness ratio of the scintillation crystal produces a detector angular response similar to that of a cosine function. At energies above about 300 keV, the angular response becomes flatter than a cosine. The LADs are uncollimated in the forward hemisphere and passively shielded as described below in the rear hemisphere.

Scintillation light from the detector crystal is viewed by three 12.7 cm photomultiplier tubes (PMTs). The signals from the three tubes are summed at the detector. The light collection technique is different from that usually used with crystal scintillation detectors. Instead of directly coupling the PMTs to the crystal window, a large light-integrating housing is used (Figure 1). The housing is lined with passive lead/tin shielding and is coated internally with a barium sulphate-based white reflector. The passive shielding is effective up to energies of about 200 keV. The front of the LAD is covered by a charged-particle detector (CPD) which uses a plastic scintillator to reject charge-particle-induced events in the LAD.

The SD is an uncollimated NaI(Tℓ) scintillation detector 12.7 cm in diameter by 7.62 cm thick. A single 12.7 cm diameter PMT is directly coupled to the scintillation detector window. The housing of the PMT has a passive lead/tin shield similar to that of the LADs. In order to provide high efficiency at energies as low as 15 keV, the

front of the crystal housing is fitted with a 7.62 cm diameter beryllium window. The axis of symmetry of an SD is offset by ~15° from the LAD axis for mechanical reasons. Since the angular response of the SD is more nearly isotropic, there is no scientific requirement for coalignment with the LAD.

Each of the eight BATSE detector modules sends data to the Central Electronics Unit (CEU) which contains hardware and software that accumulates the data into several large RAM memory areas and constructs the BATSE telemetry packet. Telemetry rate limitations require the use of a variety of data encoding and compression strategies. Extensive use of commandable parameters, plus the capability to re-program the flight software after launch, insures that BATSE will have the flexibility to respond to unforeseen conditions in orbit and/or newly discovered γ-ray phenomena.

3. DEVELOPMENT OF DETECTOR RESPONSE MATRICES

A detailed knowlege of the detector response is necessary for spectral analysis and for burst location. The response is formulated in terms of a set of matrices that characterize the detector output for a given energy input. The spectral response functions for the BATSE detectors, particularly the LADs, exhibit significant Compton tails for higher input photon energies. This effect complicates not only the photon spectral deconvolution but also the use of the LADs for reliable burst location. Furthermore, the LADs exhibit variations in light collection across the face of the crystal of ~15%, producing measurable effects on energy resolution and angular response. Several series of calibrations have been performed in order to characterize these effects with sufficient precision to meet the BATSE scientific objectives. Although only portions of the data have been analyzed in detail, it is clear that a sufficient combination of experimental data and simulations exists to assure that the desired instrument performance will be achieved.

In the remainder of this section we discuss the most important calibrations, with emphasis on the systematics of burst location using the LADs. We also briefly describe the Monte Carlo modeling and present some preliminary results of attempts to simulate the labratory calibrations. A more general discussion of the Monte Carlo methodology and the development of the BATSE response matrices may be found elsewhere.[2]

3.1. Radial response measurements

The light-integrating housing used in the BATSE LADs allows relatively uniform light collection with fewer PMTs than would be required for the more usual design in which PMTs are directly coupled to the crystal window. A radial dependence of the light collection efficiency is, however, observable and has significant consequences for detector performance. The effect is clearly evident in the shape of the full-energy peak measured during laboratory calibrations. Figure 2 is an example of the spectrum in the region of the 662 keV peak of ^{137}Cs when the full area of the detector is exposed to the source. No simple gaussian gives a good fit to the peak shape. A gaussian which provides a good fit to the high-energy side of the peak is clearly a bad fit on the low-energy side. Light collection variations would naturally produce such a response since the interactions in regions from which light collection is poor would result in a lower apparent energy.

In order to characterize the radial response, a series of measurements were performed using a collimated source to illuminate only local regions of the detector front face. As expected, the data showed that the peak response to a collimated source is fitted well by a gaussian and that the centroid of the gaussian shifts to lower pulse height as the radial position increases. The typical centroid shift near the edge is 15%.

Non-uniform light collection can in principle have both azimuthal and radial components. However, it was expected from preliminary measurements with non-flight crystals that azimuthal asymmetry would be relatively unimportant. We therefore attempted to model the peak shape by assuming azimuthal symmetry. In this case, the peak shape p as a function of energy E is given by

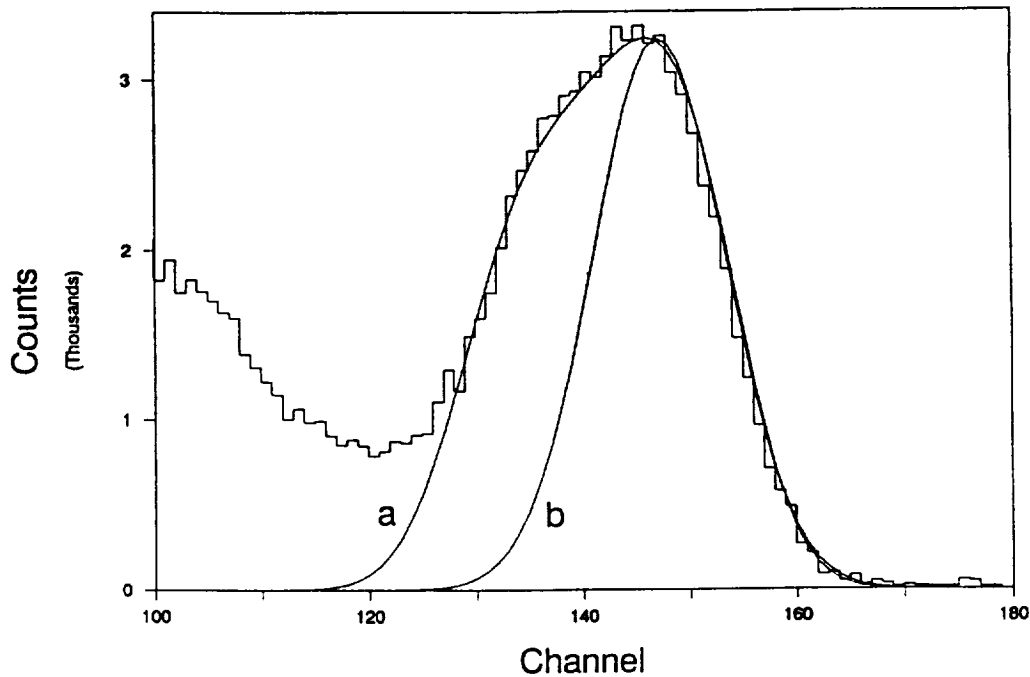$$p(E) = \int_0^R 2\pi r \exp(-\alpha(E - E_0(r))^2)\, dr. \tag{1}$$

Figure 2: The on-axis response of a typical BATSE LAD to a ^{137}Cs calibration source. Only the region near the full-energy peak is shown. The histogram represents the data. Curve a is a fit to the peak region as described in Section 3.1. Curve b is a Gaussian fit to the data at energies above the peak maximum.

Here $E_0(r)$ is the radial response (i.e., the apparent centroid energy at a distance r from the center), R is the radius of the crystal, and α is an adjustable parameter. Although the analysis is not yet complete, a simple quadratic form for $E_0(r)$ was found to give an acceptable fit to the data examined thus far. Substituting this form into Equation (1) yields a model peak shape which is then fitted to the full-energy peak data by adjusting the parameter α. The resulting shape is shown superimposed on the data in Figure 2, from which it is clear that this model is quite successful at accounting for the non-gaussian shape of the ^{137}Cs peak. Similarly good results have been obtained with line shapes from other calibration sources.

3.2. Angular response measurements

The ability of BATSE to locate γ-ray bursts results from the anisotropic angular response of the LADs. The relative efficiencies and angular response have been measured at a discrete set of energies and angles. The measurements were carried out in a high bay area in an attempt to reduce effects due to the walls and other surrounding materials. A detector module was mounted on a rotatable table such that the LAD principal axis was horizontal and perpendicular to the axis of rotation of the table. The module and table were mounted on a scaffold such that the detector was ∼5 m above the floor and ∼6 m from the nearest wall. A lead source holder/collimator was mounted at the same height on a separate scaffold located ∼12 m from the detector. Spectra were taken for each of seven sources (^{133}Ba, ^{60}Co, ^{57}Co, ^{137}Cs, ^{109}Cd, ^{75}Se, and ^{241}Am) at each of 40 different angles with respect to the LAD principal axis. Monte Carlo simulations are used to determine the response at other values of energy and/or angle.

Figure 3 is an example of the results of the angular response measurements. Shown are ^{137}Cs spectra at various angles from the principal axis of one of the LADs. The decrease in intensity as the off-axis angle increases is evident. Also noteworthy is the shift of the peak toward lower apparent energy for the nearly edge-on (96°) case. Figure 4 shows this effect more clearly. Here the measured shift is shown for two different energies as a function of the
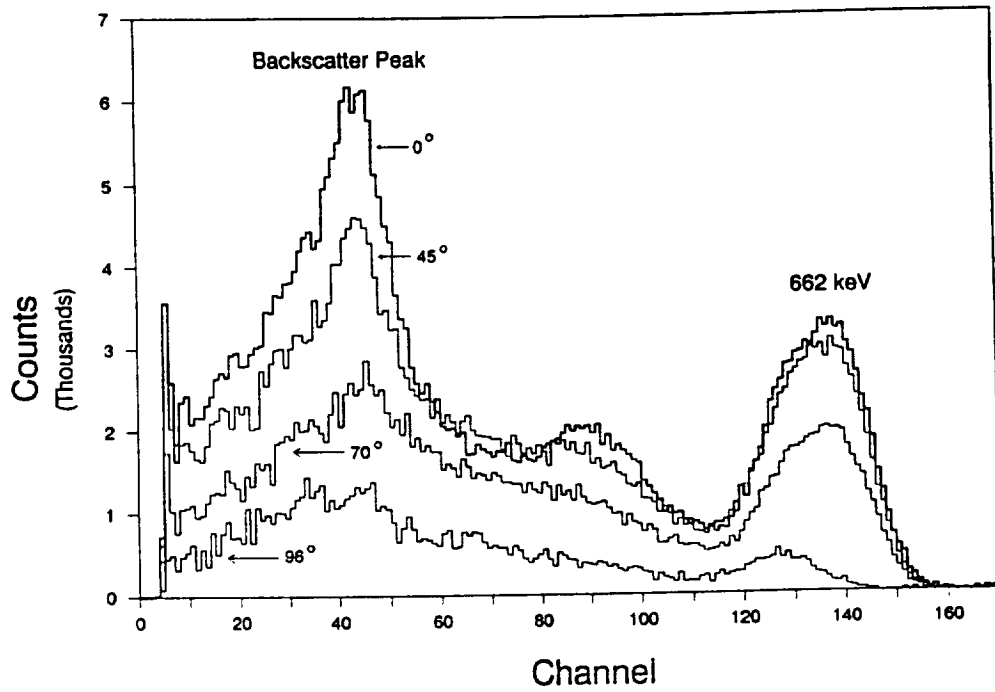
Figure 3: Measured ^{137}Cs spectra obtained at various angles of incidence relative to the LAD principal axis.
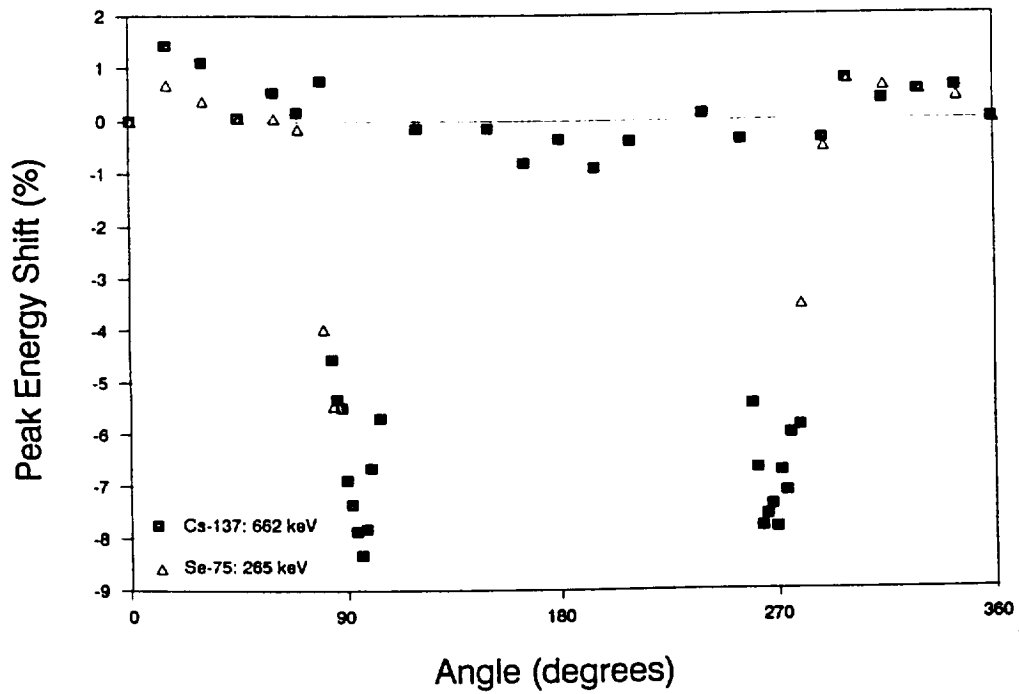

Figure 4: Measured centroid shift vs. angle of incidence for two energies. The shaded squares show data for 662 keV (^{137}Cs source) and the triangles ($\triangle$) show data for 265 keV (^{75}Se source).

incident angle. The apparent peak energy is significantly smaller for angles of incidence between ~70° and ~110°, a result which is due primarily to the radial response characteristics. At large off-axis angles the incident γ-rays interact predominantly near the edge of the crystal where the light collection is reduced relative to the center.

3.3. Monte Carlo simulations

In order to reproduce the experimental measurements with Monte Carlo calculations the detector geometry and the test environment geometry must be simulated in sufficient detail. The BATSE methodology is discussed extensively by Pendleton et al.[2] The EGS electron-photon shower code[3] is used together with a general geometry routine written by G. N. Pendleton. Detector spectra are produced by convolving the Monte Carlo energy deposition with the measured radial response and statistical broadening. Figure 5 is an example of the simulations of the data from angular response tests. Monte Carlo spectra of ^{137}Cs are shown for incident angles of 0° and 90°. The features seen in the data (Figure 3) are generally well reproduced. The notable exception is the backscatter peak near 200 keV, for which the Monte Carlo simulation produces more events on the low-energy side of the peak than are observed. These events are due to photons that scatter in the test environment before interacting in the detector. However, the spectra shown in Figure 5 were not generated with a complete representation of the angular response calibration geometry; in particular, the large lead collimator was not simulated. Other preliminary simulations which included the lead collimator have been successful in accounting for the detailed shape of the backscatter peak, and it is expected that calculations using a complete geometry will successfully simulate the entire spectrum.

3.4. Absolute efficiency calibrations

In order to measure the absolute efficiency of the detectors, nine modules (eight flight and one proto-flight) were exposed to eight different laboratory standard sources with known actvities (^{241}Am, ^{133}Ba, ^{109}Cd, ^{57}Co, ^{60}Co, ^{137}Cs, ^{203}Hg, ^{22}Na, and ^{88}Y). The sources were located far enough (≥ 280 cm) from the detectors to assure uniform illumination; the source–detector distances were measured to within ±0.05%. In contrast to the angular response calibrations, the absolute efficiency measurements were carried out in a relatively small room, so that nearby materials in the calibration environment have a larger effect on the results. The goals of the calibration were as follows:

1. Measurement of the absolute efficiencies of the LADs and SDs.

2. Measurement of the low-energy attenuation due to the presence of the thermal blankets that surround each module.

3. Verification of the Monte Carlo simulations of the detector response.

The number of photons striking the front of each LAD is determined accurately from the known source activities and the experimental geometry. The Monte Carlo simulations of the calibrations are verified by comparing both absolute intensities and spectral shapes. The success of the simulations for a representative source (^{203}Hg) is illustrated in Figure 6; here the simulations have been normalized to the data solely on the basis of the source activity.

More than 99% of the events in the ^{203}Hg full-energy peak are due to photons that enter the LAD directly without scattering in any of the surrounding material. In the Monte Carlo simulations, no arrangement of materials in the test environment produces a significant contribution to the full-energy peak from photons scattering in the test environment before interacting in the detector. Therefore, comparison of the counts in the measured and simulated full-energy peaks yields an accurate assessment of the absolute detection efficiency. It is clear from Figure 6 that the absolute efficiency is adequately understood.

In the absolute efficiency calibrations the sources were not collimated, so that scattering off objects in the test environment has a more significant effect than for the angular response measurements. Since simulation of all
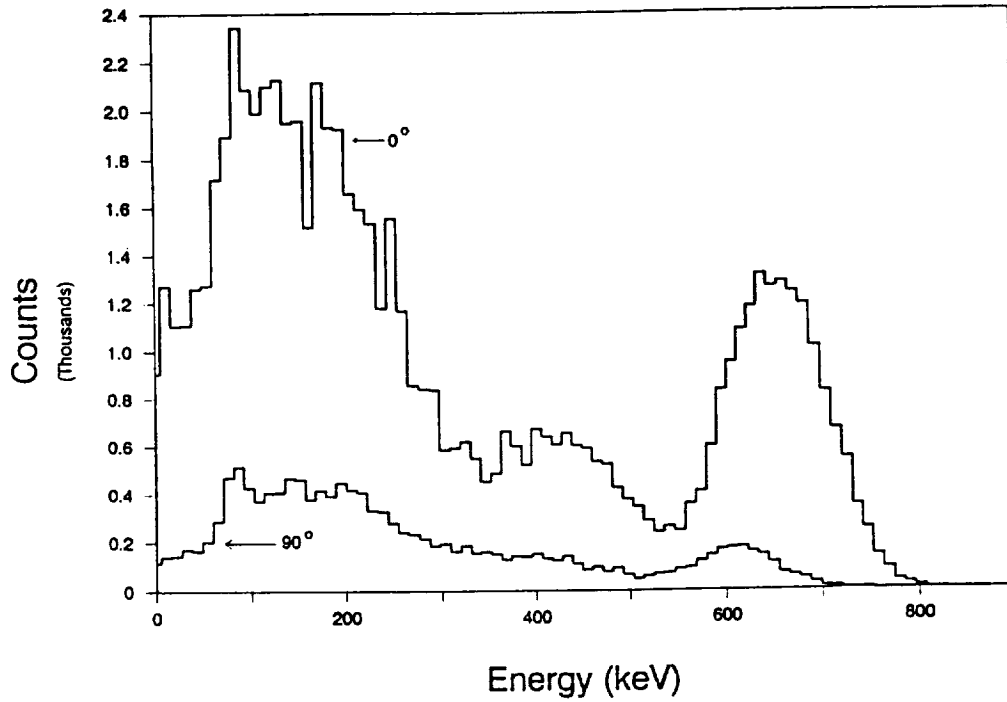
Figure 5: Spectra produced by Monte Carlo simulations of the LAD exposed to a ^{137}Cs source in the Angular Response Test geometry. Spectra for 0° and 90° incidence are shown. The axes have not been normalized to the measured spectra (Figure 3).
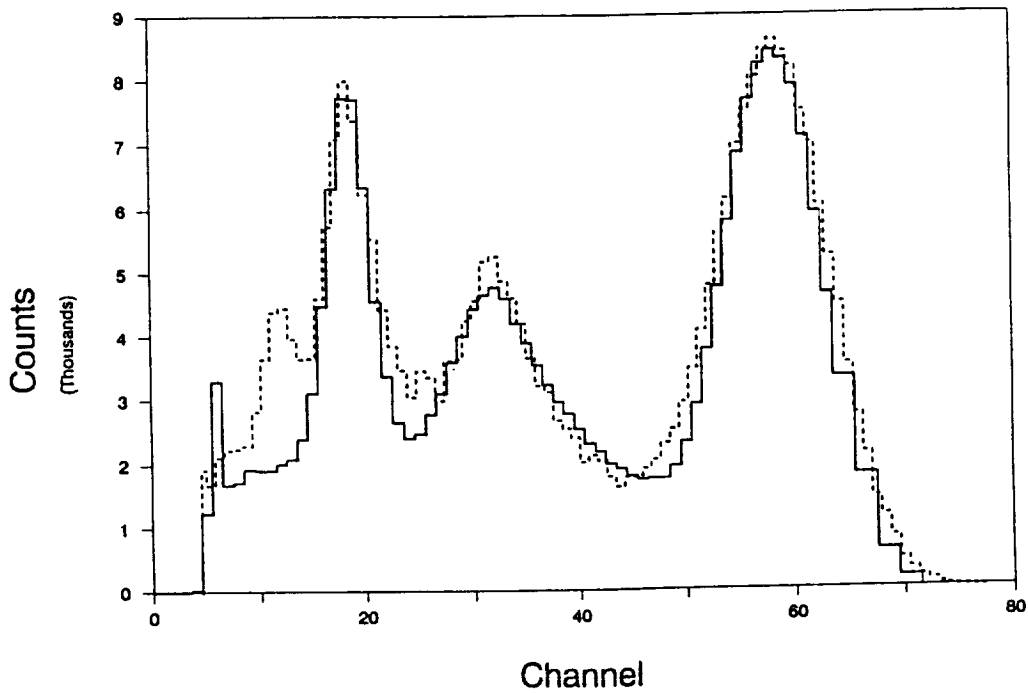

Figure 6: Comparison of measured and simulated spectra of a ^{203}Hg source taken during the LAD absolute efficiency calibrations. The solid histogram represents the data; the dashed histogram represents the simulations.

BATSE Burst Location Uncertainties

Source of Error		$\Delta\theta$
Systematic		
	Detector Efficiences & Calibration	0.4°
	Detector Alignment & Aspect uncertainty	0.2°
	Spacecraft Scattering	0.4°
	Atmospheric Scattering	0.4°
	Subtotal (RMS)	0.7°
Statistical	(Burst size)	
	10^{-7} erg·cm^{-2}	26°
	10^{-6} erg·cm^{-2}	3°
	10^{-5} erg·cm^{-2}	0.4°
	10^{-4} erg·cm^{-2}	0.1°

Table 1: Estimated burst location accuracy

objects is impractical, simplified approximations were used in the simulations. which were designed to show only that the total number of events in the backscatter region could be accounted for.

The effect of the thermal blankets on the spectrum was also determined in the absolute efficiency calibrations. Comparisons of total energy deposited in each detector with and without the thermal blankets verified that the blankets have less than 1% effect on the absolute efficiency over most of the LAD energy range.

4. CAPABILITIES FOR BURST LOCATION

The directions to burst sources will be determined by comparing relative counting rates among the LADs. The concept of using several detectors with anisotropic angular response for determining burst locations was first elaborated by Golenetskii et al.[4] For sufficiently strong bursts, the accuracy of the locations thus obtained is limited by various systematic errors. Table 1 summarizes the estimated BATSE burst location uncertainties. Uncertainties in detector response determination are estimated to result typically in a location uncertainty of 0.4°. It is expected that scattering from the GRO spacecraft and the Earth's atmosphere will also be determined well enough to contribute a similar amount to the location uncertainty.

Radiation scattering from the spacecraft normally enters the LAD from behind. Although the light collection cones include some passive lead/tin shielding which reduces this component at low energies, this component is expected to be a significant source of error in burst locations. In order to characterize the effect, measurements of spacecraft scattering using radioactive sources were performed after instrument integration at TRW. The measurements will be supplemented by Monte Carlo calculations which use a detailed mass model of the GRO spacecraft. This should allow reduction of the systematic error due to spacecraft scattering to 0.4° for the typical burst.

Scattering of burst photons in the Earth's atmosphere is also a significant source of systematic uncertainty. This effect is much larger than spacecraft scattering, but can be simulated more easily in this case because of the well-known geometry and composition of the atmosphere. The uncertainty is strongly dependent on the elevation of the burst above the Earth's limb; a value of 0.4° is expected to be attainable for the typical burst. Extensive Monte Carlo modeling of atmospheric scattering has been performed previously.[5] Further studies are planned.

The total systematic error is expected to be somewhat less than 1° for the typical burst. A number of approaches

will be used in orbit to confirm the response determination and to reduce systematic errors further. With eight detectors the location is overdetermined. Since each burst is observed directly by four detectors, while only three are needed to compute a location, an estimate of the systematic error is available for each burst. Detectors facing away from the burst, but facing the atmosphere, will provide measurements of atmospheric scattering. Systematic corrections can be improved by using independently-located bursts such as solar flares, bursts located by the interplanetary network, and possibly even orbiting nuclear reactors.

Statistical errors as a function of burst fluence are also provided in Table 1, which indicates that BATSE should be able to determine locations to better than $1°$ for bursts larger than about 10^{-5} erg-cm^{-2} (*i.e.*, several dozen bursts per year).

5. SUMMARY

The BATSE detectors have been subjected to intensive testing and calibration in order to assure that systematic errors will not compromise the instrument's scientific objectives. In combination with detailed Monte Carlo simulations, the calibrations can and will be used to develop the detector response matrices necessary for reliable γ-ray burst location.

6. ACKNOWLEDGEMENTS

REFERENCES

1. G. J. Fishman, C. A. Meegan, R. B. Wilson, W. S. Paciesas, T. A. Parnell, R. W. Austin, J. R. Rehage, J. L. Matteson, B. J. Teegarden, T. L. Cline, B. E. Schaefer, G. N. Pendleton, F. A. Berry, Jr., J. M. Horack, S. D. Storey, M. N. Brock and J. P. Lestrade, "BATSE: The Burst and Transient Source Experiment on the Gamma Ray Observatory," paper presented at the Gamma Ray Observatory Science Workshop, Greenbelt, MD, 10-12 April, 1989.

2. G. N. Pendleton, W. S. Paciesas, J. P. Lestrade, G. J. Fishman, R. B. Wilson and C. A. Meegan, "The BATSE Detector Response Matrices," paper presented at the Gamma Ray Observatory Science Workshop, Greenbelt, MD, 10-12 April, 1989.

3. R. L. Ford and W. R. Nelson, "The EGS Code System: Computer Programs for the Monte Carlo Simulation of Electromagnetic Cascade Showers," *SLAC Report no. 210*, June 1978.

4. S. V. Golenetskii, V. N. Il'inskii and E. P. Mazets, "Determination of the Efficiency and Angular Directivity of Cosmic γ-Ray Detectors," *Cosmic Research*, vol. 12, pp. 706-712, 1975.

5. D. J. Morris, "Monte Carlo Simulation of Atmospheric Gamma-Ray Scattering," *High Energy Transients in Astrophysics*, ed. Stanford E. Woosley, pp. 665-668, AIP, New York, 1984.

Appendix B

Some Results from Atmospheric Scattering Simulations

G. N. Pendleton and F. E. Roberts

ABSTRACT

We will present here some preliminary results of the atmospheric scattering simulations run to date with the EGS3 code and a spherical geometry routine tailored to the modeling of the earth's atmosphere. One of the main points of this report is to emphasize the importance of the contribution of multiple scattering events to the total observed atmospheric scattering. Details concerning the final product of this simulation project will be described in a future report.

1.   Introduction

In this report the geometry of the atmospheric model is described as well as the specific photon input parameters and collection methods used to date. The results emphasize the significant contribution of multiply-scattered photons to the total observed scattered photon flux. Multiply-scattered photons are are those that have compton scattered more than once before reaching the GRO altitude. Energy spectra for singly-scattered photons and multiply-scattered photons are presented for different photon input energies and latitudes. The techniques to be employed in the construction of the final atmospheric scattering product will not be addressed here but will be described in detail in a future report.

2.   Simulation Geometry and and Photon Input and Output Characteristics

The simulation of the earth's atmosphere is contained within a geometry consisting of 20 concentric spherical shells. 14 of these spherical shell volumes span the range in radius from 6395 km to 6878 km and represent the Earth's atmosphere from an altitude of 17 km to 500 km. The air density within each shell is constant but drops off rapidly as the successive shell radii increase in accordance with the COSPAR International

Reference Atmosphere[1]. The additional shells lying beneath the atmosphere consist of very dense air. These regions may be used if a more accurate approximation to the change in density with radius of the atmosphere is desired.

The collection surface for scattered photons is a spherical shell at an altitude of 450 km above the earth's surface. This surface is depicted in figure 1 by a set of horizontal circles each of constant latitude. Here latitude is 0° at the poles and 90° at the equator. In figure 1 there is a ray of 250 kev photons intersecting the atmospheric model at a latitude of 60°. The latitude of a ray of photons is defined by the angle between the vector through the earth's poles and a vector from the origin through the point at which the ray of photons intersects the collection surface as shown in figure 1.

The photons scatter and are collected at the collection surface. At that point the photon's energy, position, direction, and the number of scatters suffered by that photon are output to file. Figure 2 shows a close up of the trajectories of scattered photons intersecting the collection surface. The paths of these trajectories demonstrate that a significant fraction of these photons have scattered more than once before intersecting the collection surface. Figure 3, which shows the distribution of photons versus the number of scatters suffered by the photon before intersecting the collection sphere, supports this conclusion as well.

Figure 4 presents the distribution of latitudes at which the scattered photons were collected. At this incident latitude(60°) most of the collected photons have been scattered forward to higher latitudes. Figure 5 shows the energy distribution of the collected photons summed over all collection latitudes and all collected photon directions. There is a spike in this spectrum a little above 126 kev. Since the minimum energy a 250 keV photon can have after one scattering(180°) is 126.36 keV, this spike represents the end of the single scattering contribution to the collected photon energy distribution.

The photon direction is defined by a zenith angle θ and an azimuthal angle ϕ. The zenith angle is measured from an axis aligned along the radial vector passing through the point at which the particle is collected. ϕ is defined as 0° along a vector whose base is at the axis of the earth and whose tip touches the radial zenith vector. Figures 6 and 7 show the θ and ϕ distributions respectively of the collected photons. The θ distribution shows a cutoff before 90° due to higher absorption and the small probability of a photon moving nearly parallel to a surface intersecting that surface. The azimuthal distribution is fairly isotropic with a slight peak in the $\phi = 0°$ direction due to single forward scattering.

3. Energy Distributions of Collected Photons

In this section histograms of the energy distributions of collected photons produced by monoenergetic incident rays of photons input at specific latitudes will be presented. These photons are summed over all collection latitudes and collected photon directions. There are two histograms on each plot. The solid line histogram represents the energy spectrum of photons that have suffered only a single scatter before collection. The dotted line histogram represents the spectrum of multiply-scattered collected photons.

The first series of plots, figures 8A through 8F, represent the scattered flux due to 250 keV photons input at latitudes ranging from 0° to 70°. Photons input at a latitude of 75° produced no scattered flux since they did not intercept the denser parts of the atmosphere. Both the singly and multiply-scattered fluxes show an increase in their higher energy components with increasing latitude. This is not surprising since forward scattering photons can hit the collection surface at higher latitudes. The lower energy component of the multiply-scattered flux does not exhibit as much of a latitude dependence as the higher energy component. Also preliminary analysis of the scattered photon direction results indicate that this component is more isotropic than the higher energy component of either the singly or multiply-scattered flux. It may turn out that this component tends to significantly effect the atmospheric scattering corrections to the BATSE LAD's.

Figures 9A through 9G show the singly and multiply-scattered fluxes obtained for photons with a variety of energies input at a latitude of 60°. These results show that the multiply-scattered flux is a significant component of the total observed flux over the energy range from 50 keV to 750 keV. There is also a strong component in the multiply-scattered fluxes between 50 keV and 100 keV for all incident energies above 100 keV. This particular component seems relatively insensitive to variations in latitude and incident energy and may result in some ill-conditioned response matrices when those matrices require large corrections for atmospheric scattering.

Finally table 1 shows the percentages of singly and multiply-scattered photons for all the runs presented in figures 8A through 9G. These results show that the multiply-scattered component is generally equal to or greater than the singly-scattered component. Hence analytic atmospheric scattering corrections that only take single scattering and some reduced absorption effect into account may not produce the right modifications to the response matrices.

Comparisons between the results generated with the present code and single scattering codes will be performed. Also comparisons with Dan Morris's monte carlo data will be performed. When these comparisons have been made and the basic structure of the atmospheric correction algorithm we are developing has been ironed out another report will be made.

1. **High Energy Astrophysics Handbook**, Martin v. Zombeck,
Smithsonian Astrophysical Observatory Special Report 386, 1980
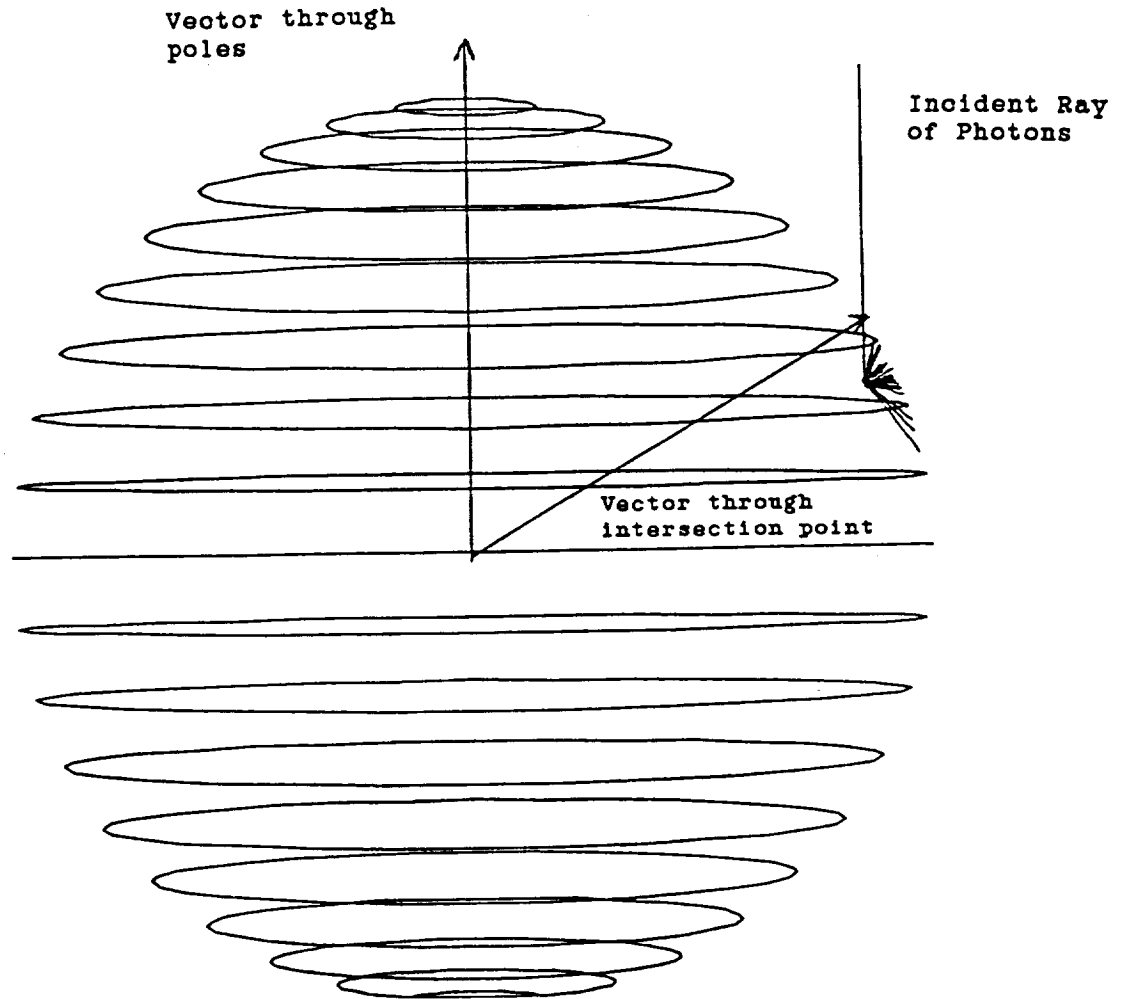
Figure 1: Earth's Atmosphere Model

Vector through
poles

Incident Ray
of Photons

Vector through
intersection point

Figure 2: Close Up of Scattered Trajectories
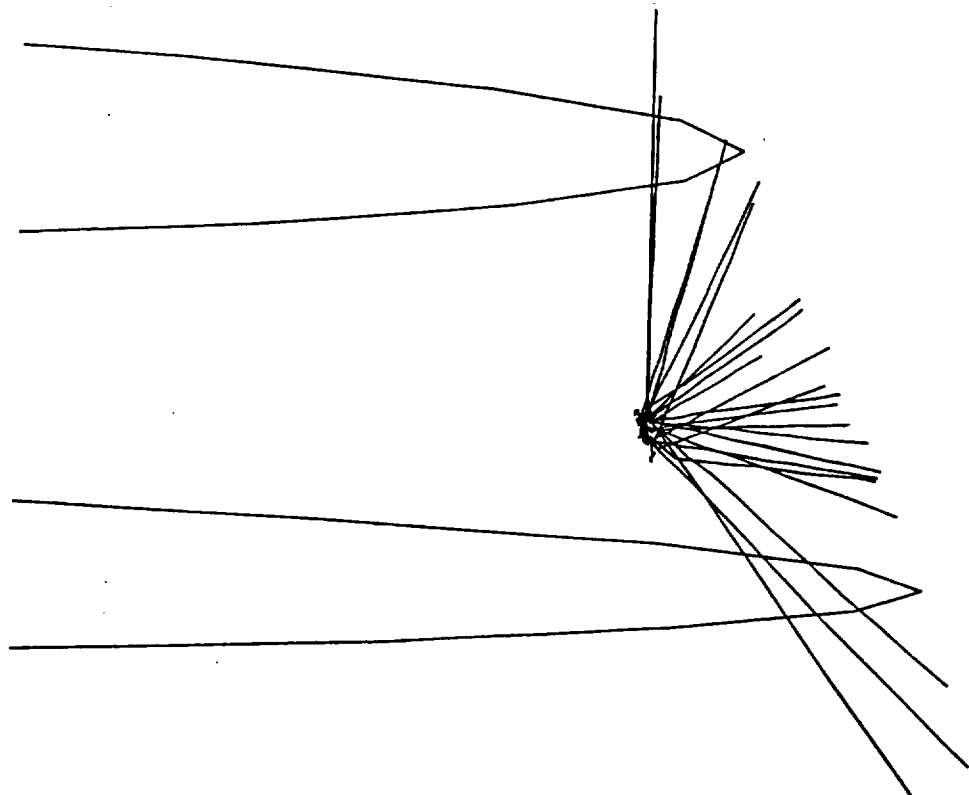
Figure 3: Histogram of Number of Scatters per Photon

Incident Energy: 250 keV

Incident Latitude: 60 degrees
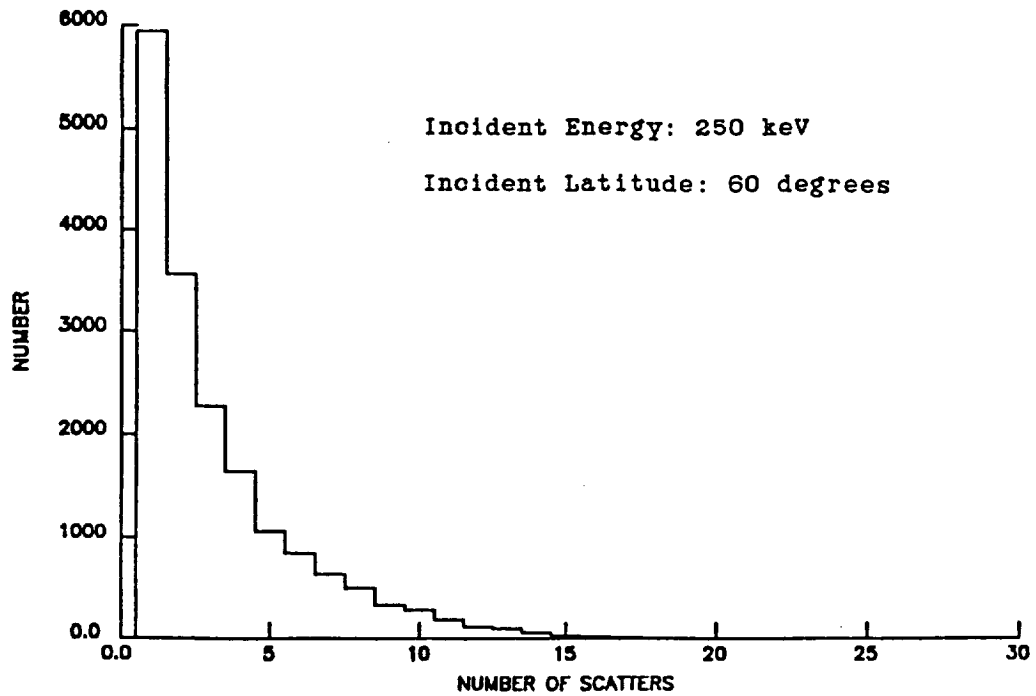
Figure 4: Latitude distribution of Collected Photons

Incident Energy: 250 keV

Incident Latitude: 60 degrees
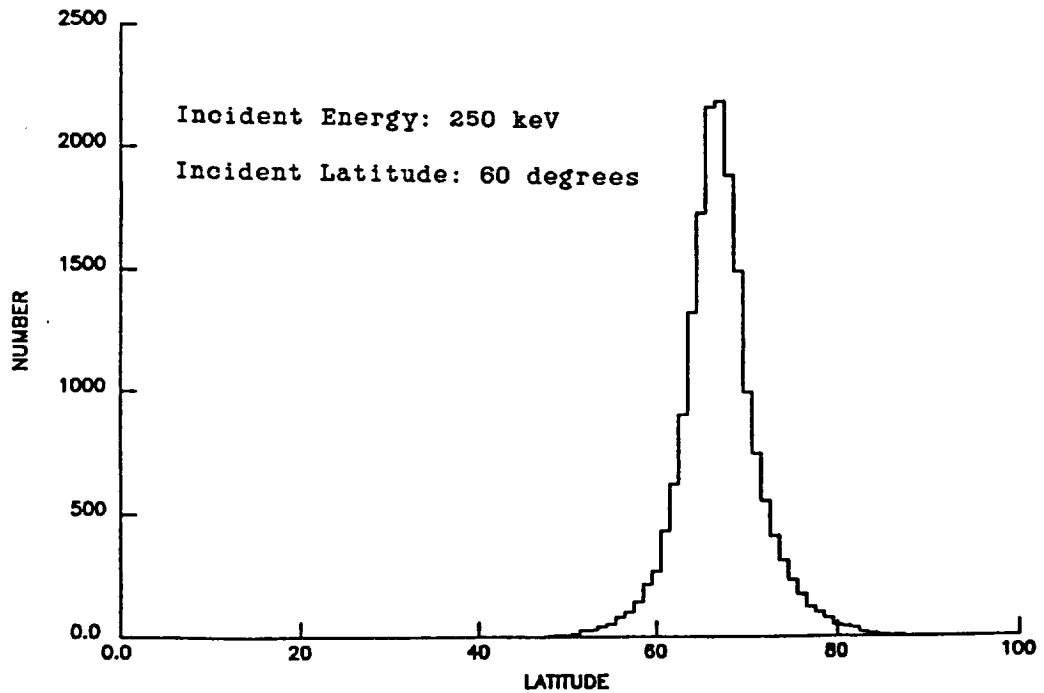
Figure 5: Energy Distribution of Collected Photons

Incident Energy: 250 keV

Incident Latitude: 60 Degrees
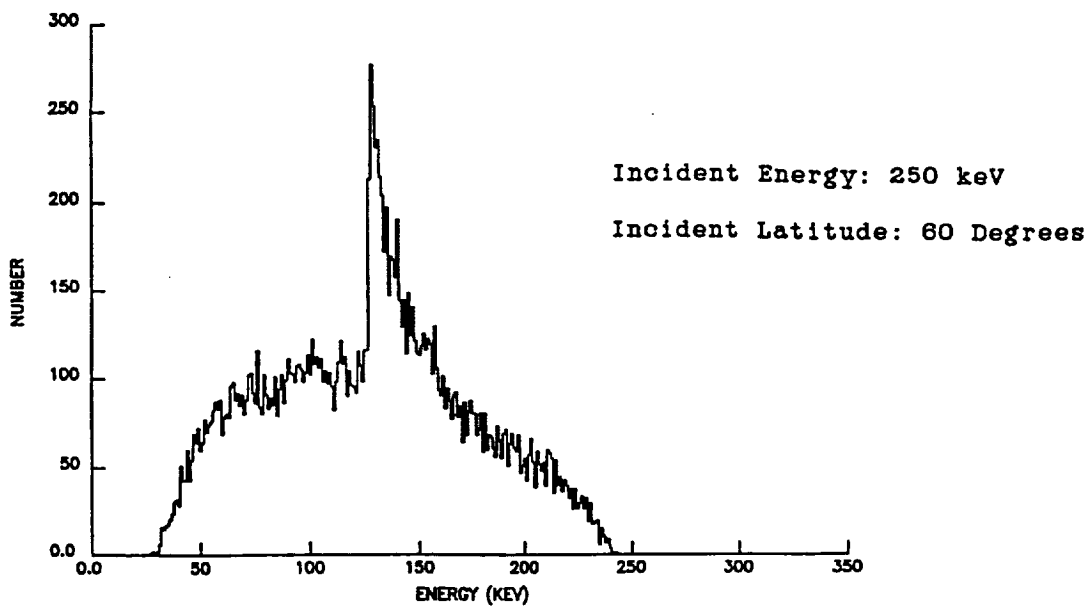
Figure 6: Zenith Angle Distribution of Collected Photons

Incident Energy: 250 keV

Incident Latitude: 60 Degrees
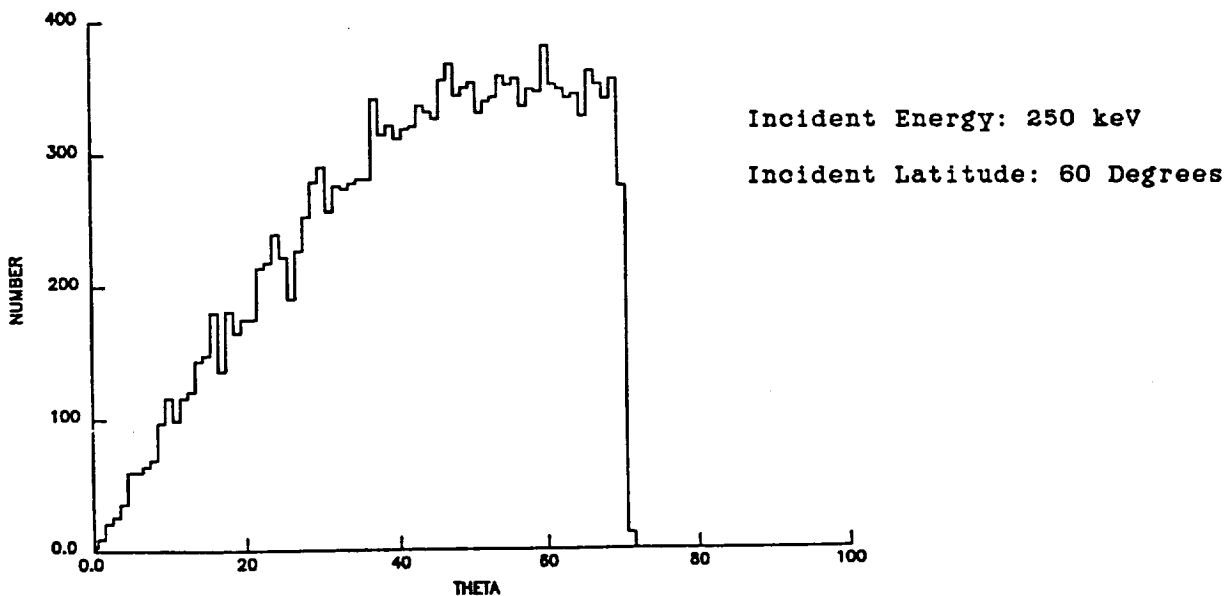
Figure 7: Azimuthal Angle Distribution of Collected Photons

Incident Energy: 250 keV

Incident Latitude: 60 Degrees
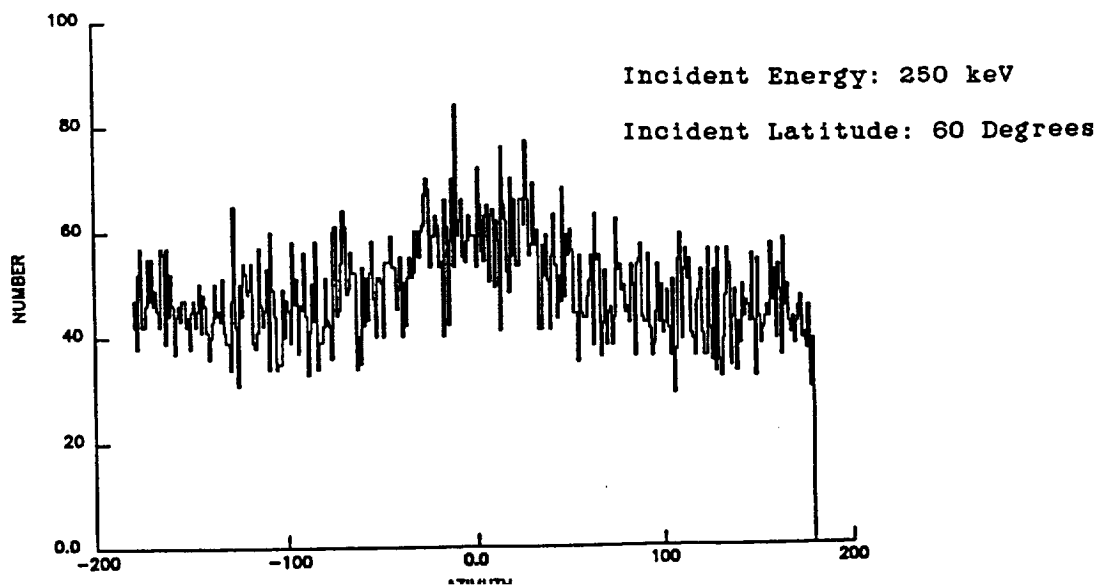
Figure 8A: Energy Spectra of Collected Photons

SINGLE SCATTERS

MULTIPLE SCATTERS

Incident Energy: 250 keV

Incident Latitude: 0 Degrees

NUMBER

ENERGY (KEV)
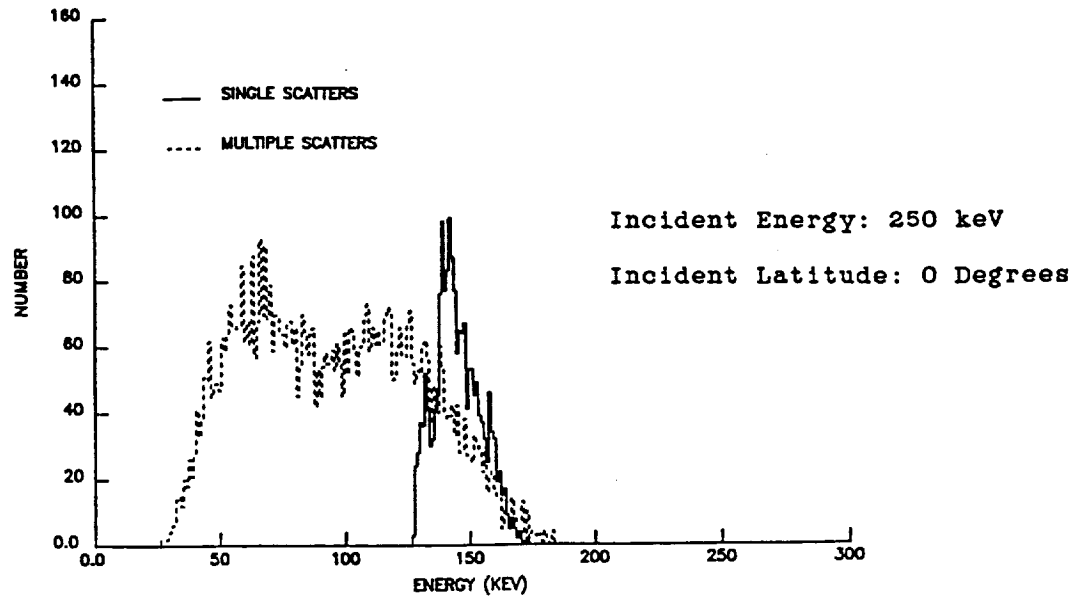
Figure 8B: Energy Spectra of Collected Photons

SINGLE SCATTERS

MULTIPLE SCATTERS

Incident Energy: 250 keV

Incident Latitude: 15 Degrees

NUMBER

ENERGY (KEV)
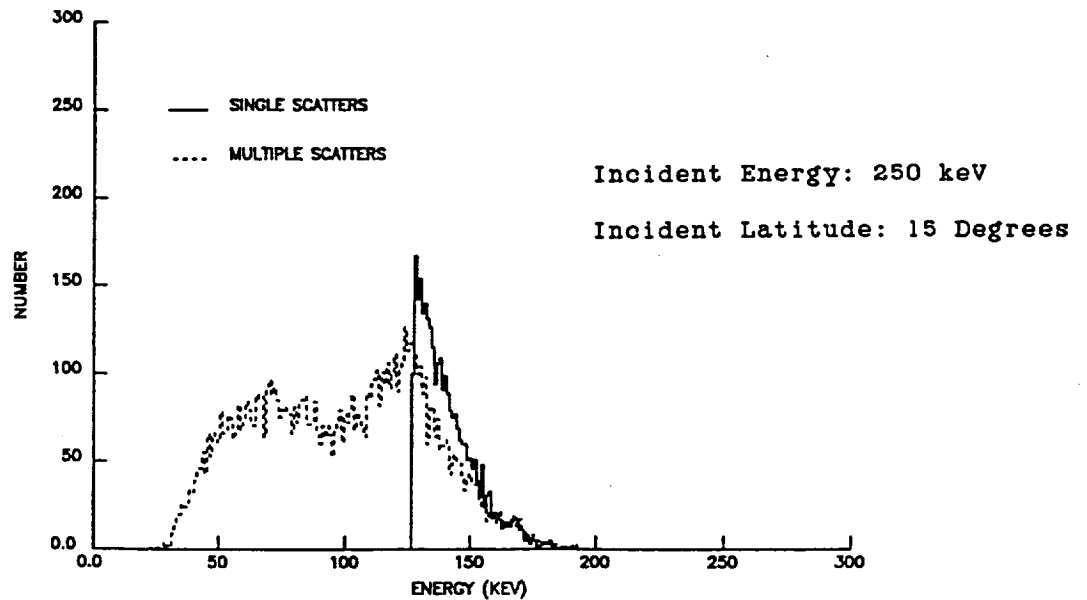
Figure 8C: Energy Spectra of Collected Photons

SINGLE SCATTERS

MULTIPLE SCATTERS

Incident Energy: 250 keV

Incident Latitude: 30 Degrees

NUMBER

ENERGY (KEV)
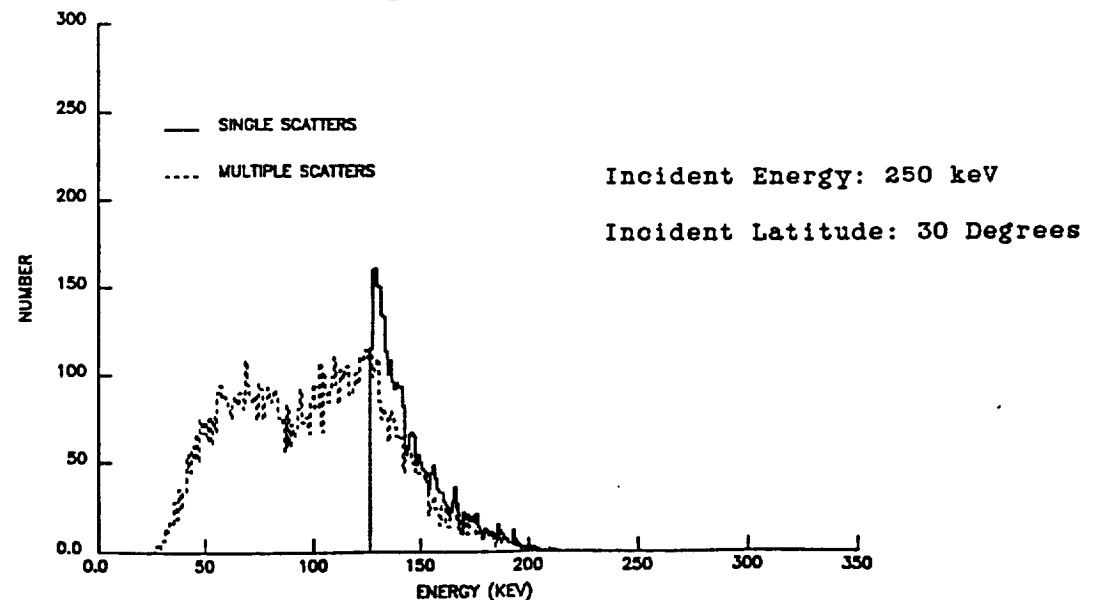
Figure 8D: Energy Spectra of Collected Photons

SINGLE SCATTERS

.... MULTIPLE SCATTERS

Incident Energy: 250 keV

Incident Latitude: 45 Degrees
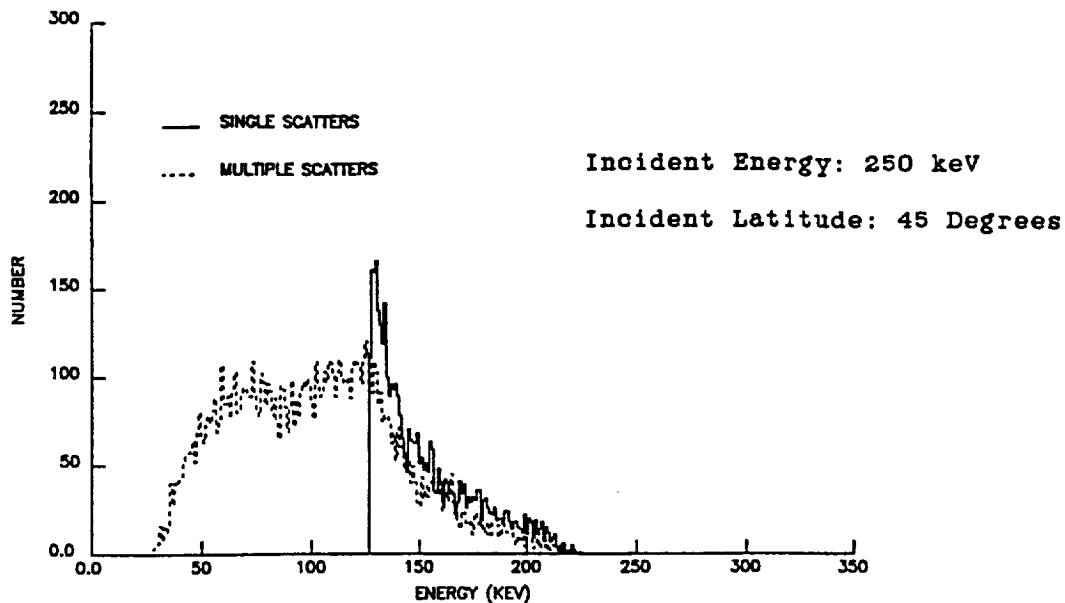
Figure 8E: Energy Spectra of Collected Photons

SINGLE SCATTERS

.... MULTIPLE SCATTERS

Incident Energy: 250 keV

Incident Latitude: 60 Degrees
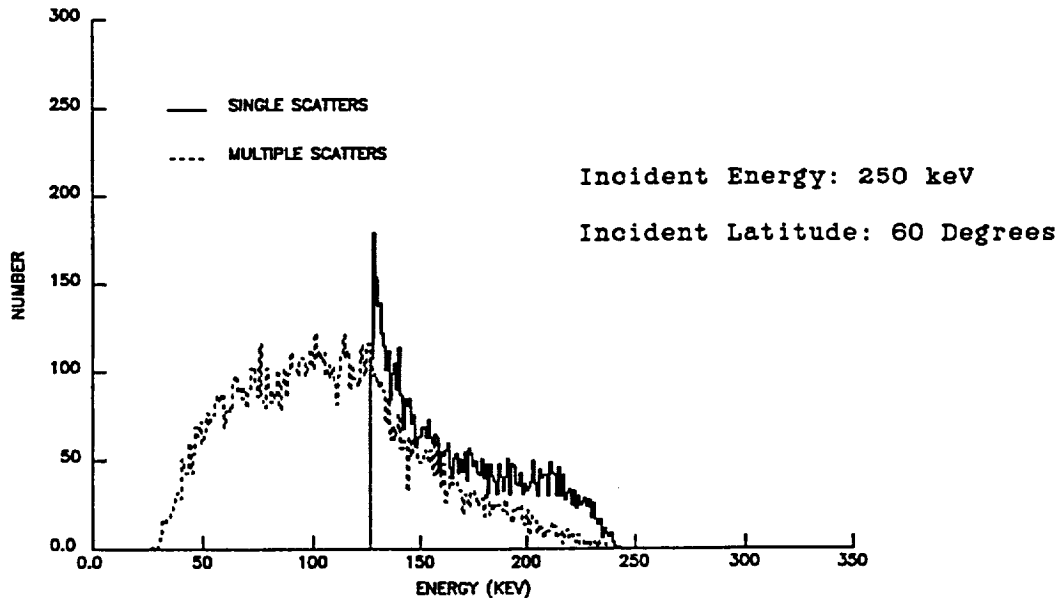
Figure 8F: Energy Spectra of Collected Photons

SINGLE SCATTERS

.... MULTIPLE SCATTERS

Incident Energy: 250 keV

Incident Latitude: 70 Degrees
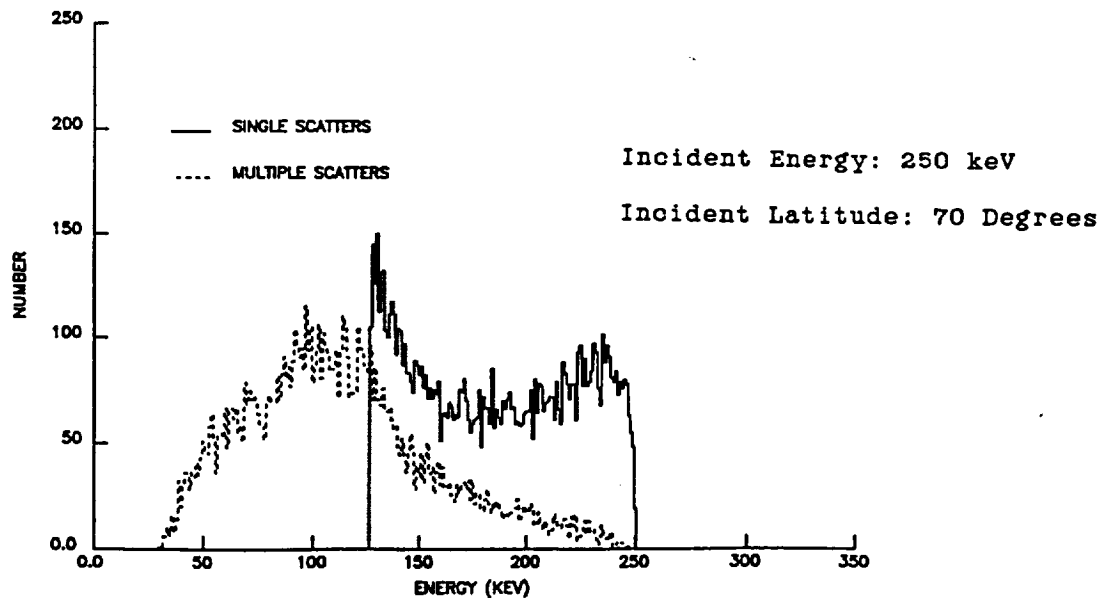
Figure 9A: Energy Spectra of Collected Photons

SINGLE SCATTERS

.... MULTIPLE SCATTERS

Incident Energy: 50 keV

Incident Latitude: 60 Degrees
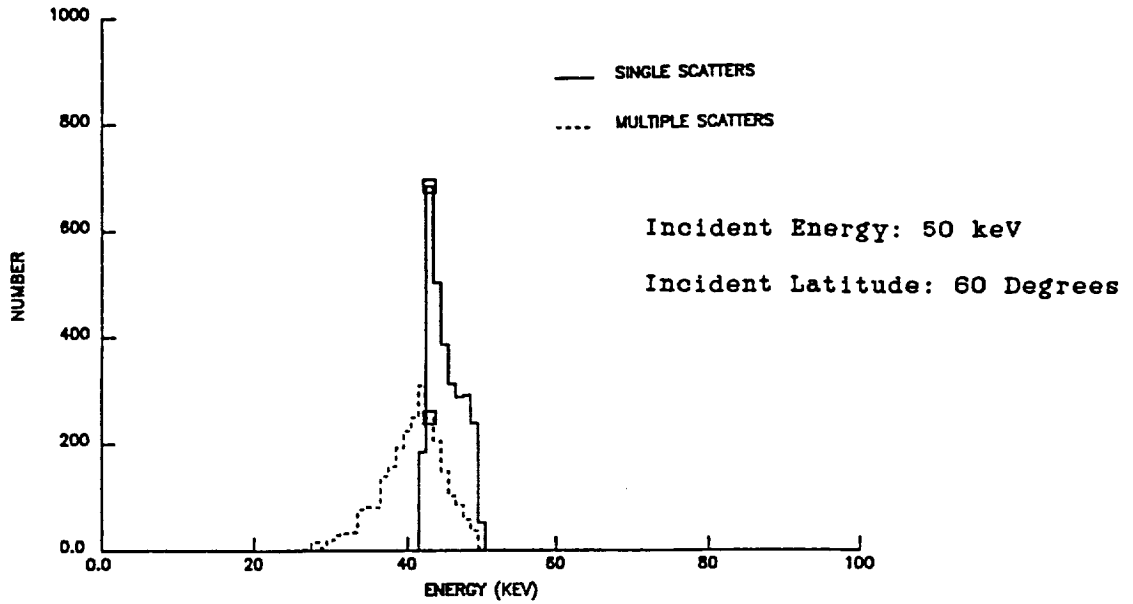
Figure 9B: Energy Spectra of Collected Photons

SINGLE SCATTERS

.... MULTIPLE SCATTERS

Incident Energy: 100 keV

Incident Latitude: 60 Degrees
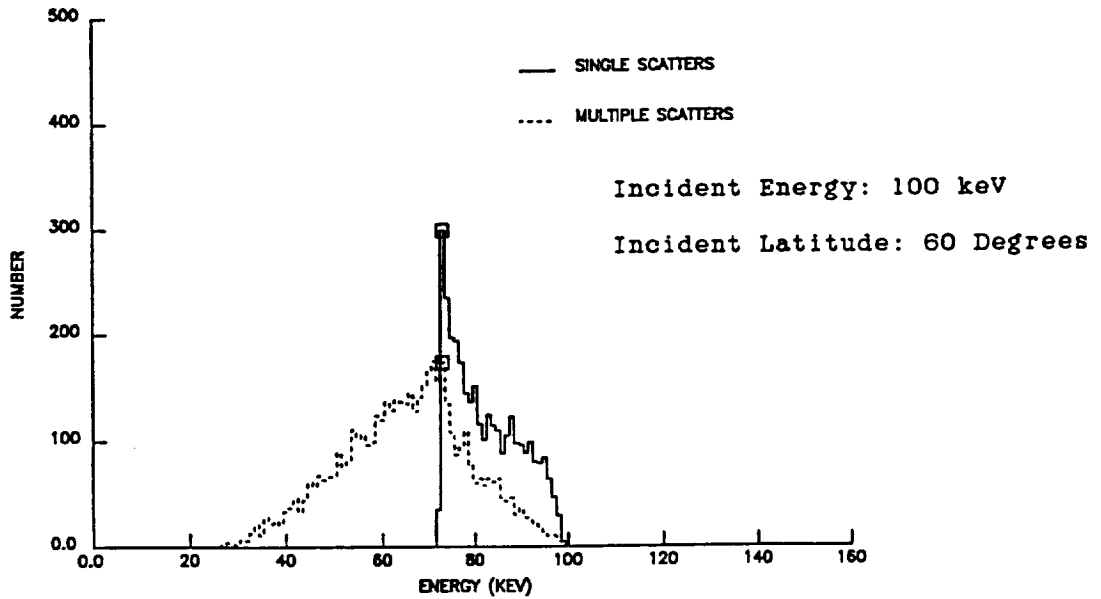
Figure 9C: Energy Spectra of Collected Photons

SINGLE SCATTERS

.... MULTIPLE SCATTERS

Incident Energy: 150 keV

Incident Latitude: 60 Degrees
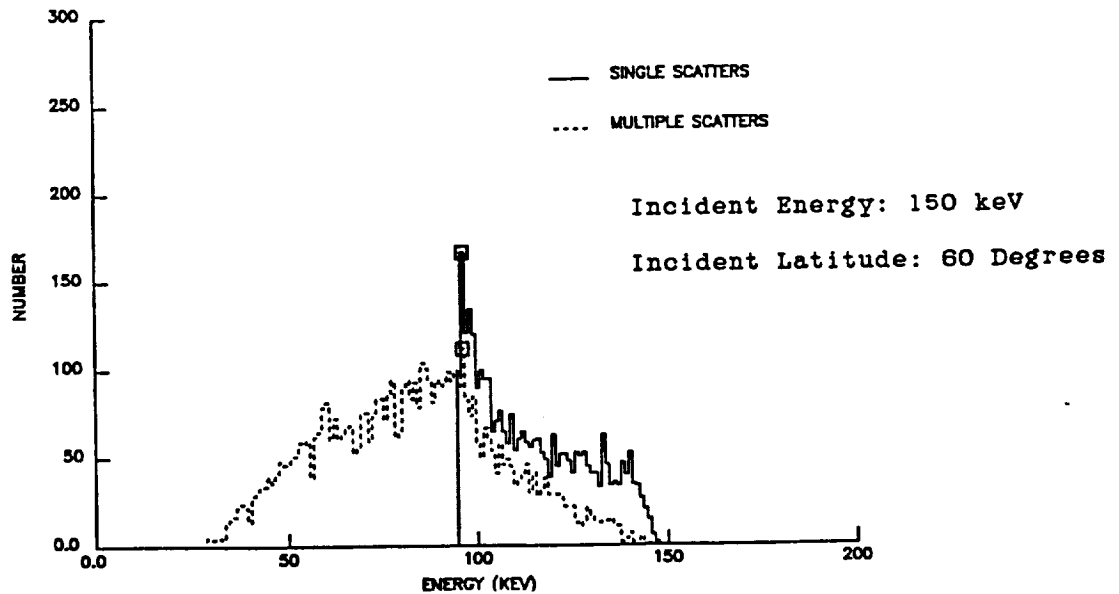
Figure 9D: Energy Spectra of Collected Photons

SINGLE SCATTERS

.... MULTIPLE SCATTERS

Incident Energy: 200 keV

Incident Latitude: 60 Degrees
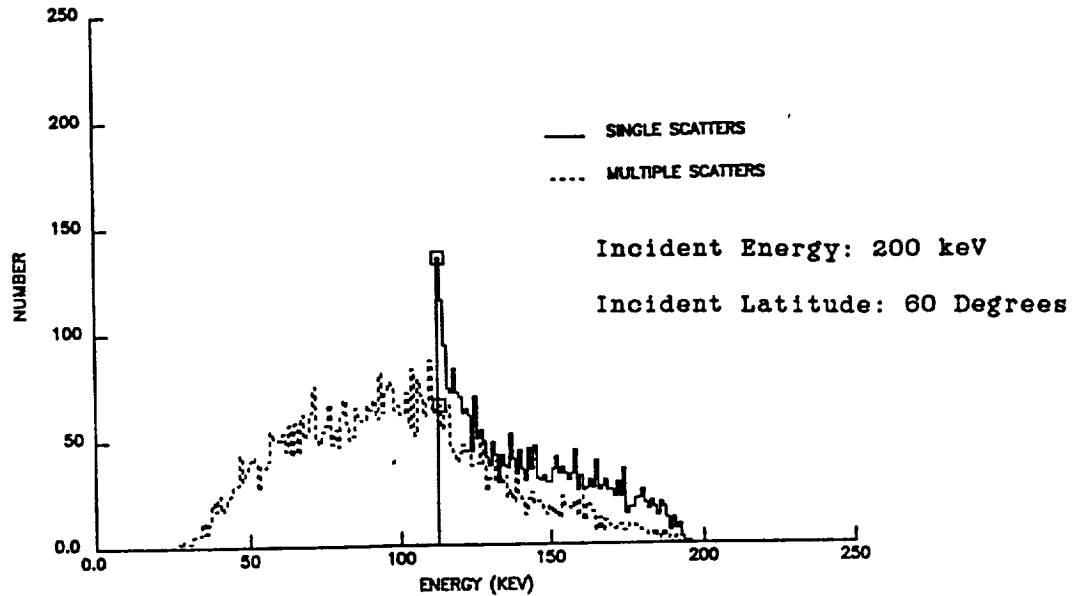
Figure 9E: Energy Spectra of Collected Photons

SINGLE SCATTERS

.... MULTIPLE SCATTERS

Incident Energy: 350 keV

Incident Latitude: 60 Degrees
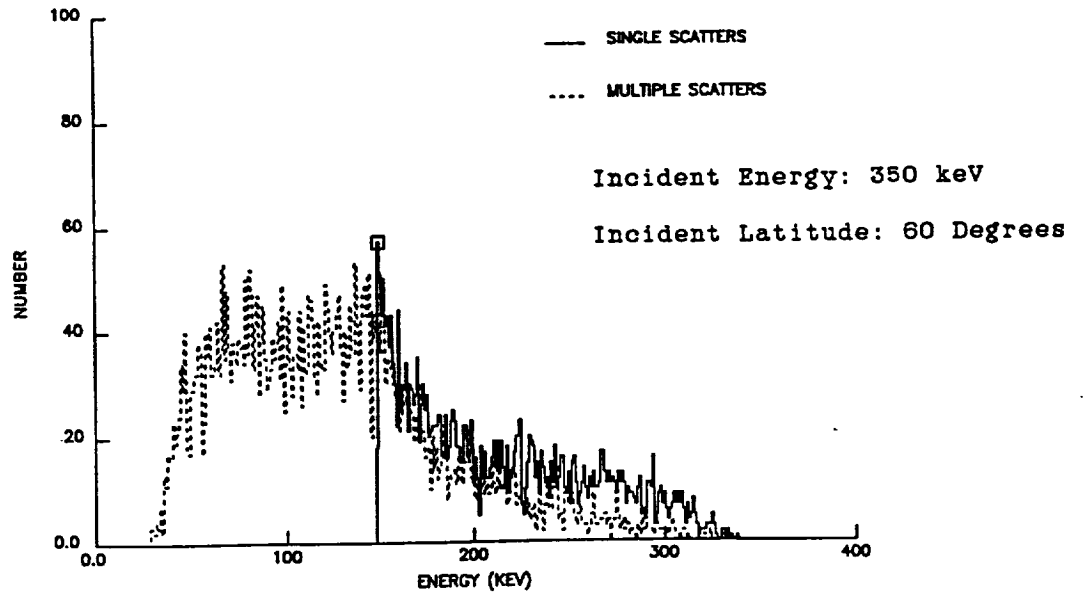
Figure 9F: Energy Spectra of Collected Photons

SINGLE SCATTERS

.... MULTIPLE SCATTERS

Incident Energy: 511 keV

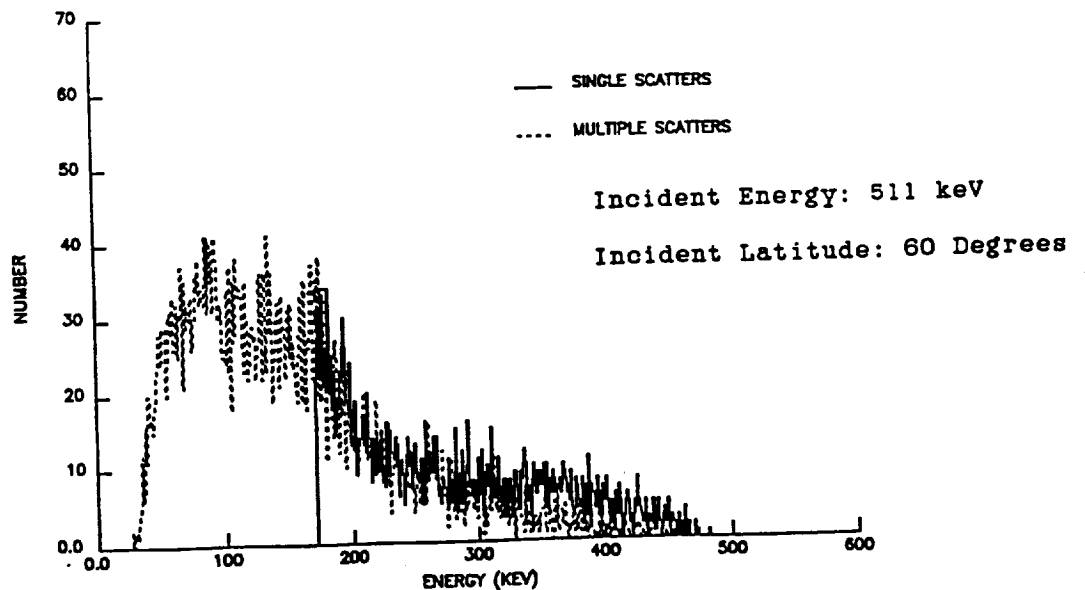Incident Latitude: 60 Degrees

Figure 9G: Energy Spectra of Collected Photons
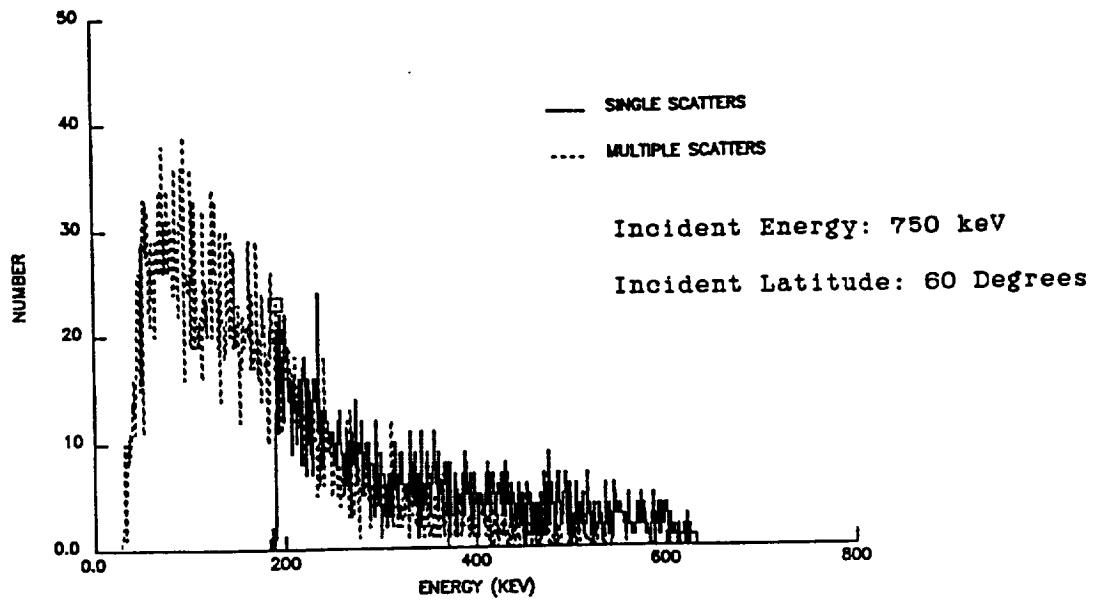
TABLE 1

Incident Energy (keV)	Incident Latitude (degrees)	Single Scatter Percentage	Multiple Scatter Percentage
250	0	20.9 %	79.1 %
250	15	24.5 %	75.5 %
250	30	25.1 %	74.9 %
250	45	27.7 %	72.3 %
250	60	33.9 %	66.1 %
250	70	50.4 %	49.6 %
50	60	53.7 %	46.3 %
100	60	39.3 %	60.7 %
150	60	35.9 %	64.1 %
200	60	34.4 %	65.6 %
350	60	32.3 %	67.7 %
511	60	31.0 %	69.0 %
750	60	32.6 %	67.4 %

Appendix C

Hard X-Ray Continuum Spectra of SN1987A

G.N. Pendleton,W.S. Paciesas(UAH),R.B. Wilson,
G.J. Fishman,C.A. Meegan(NASA/MSFC)

Supernova 1987A hard X-ray continuum spectra obtained
on Oct. 29, 1987, Apr. 9-10, 1988, and Nov. 2, 1988
on balloon flights of modified BATSE detectors are
presented in the energy range from 25 keV to 300 keV.
The spectral reconstruction techniques applied to the
three flight's data are described. Crab Nebula spectra
obtained on these flights and analyzed using the same
techniques are presented. Comparisons between our data
and the spectra predicted by theoretical models at
the times of our three observations will be presented.

NASA

Report Documentation Page

1. Report No.	2. Government Accession No.	3. Recipient's Catalog No.

4. Title and Subtitle	5. Report Date
Final Report "Gamma Ray Astronomy"	January 14, 1991
	6. Performing Organization Code

7. Author(s)	8. Performing Organization Report No.
William S. Paciesas	
	10. Work Unit No.

9. Performing Organization Name and Address	11. Contract or Grant No.
The University of Alabama in Huntsville, AL 35899	NAS8-36955, D. O. 42
	13. Type of Report and Period Covered

12. Sponsoring Agency Name and Address	Final July 13, 1989-January 12, 1991
George C. Marshall Space Flight Center National Aeronautics & Space Administration Marshall Space Flight Center, AL 35812	14. Sponsoring Agency Code

15. Supplementary Notes

16. Abstract

Miscellaneous tasks related to the development of the Burst and Transient
Source Experiment on the Gamma Ray Observatory and to analysis of archival
data from balloon flight experiments were performed. The results are summarized
and relevant references are included.

17. Key Words (Suggested by Author(s))	18. Distribution Statement
Gamma-ray Astronomy	Unclassified-Unlimited

19. Security Classif. (of this report)	20. Security Classif. (of this page)	21. No. of pages	22. Price
		32	

DISPLAY 91N26407/2

91N26407*   ISSUE 18   PAGE 2972   CATEGORY 32
RPT#: NASA-CR-184409 NAS 1.26:184409   CNT#: NAS8-36955   91/01/00   33
PAGES   UNCLASSIFIED DOCUMENT
UTTL: Gamma ray astronomy   TLSP: Final Technical Progress Report, 13 Jul. 1989
      -- 12 Jan. 1991
AUTH: A/PACIESAS, WILLIAM S.
CORP: Alabama Univ., Huntsville.   CSS: (Dept. of Physics.)
SAP: Avail: CASI HC A03/MF A01
CIO: UNITED STATES
MAJS: /*GAMMA RAY ASTRONOMY/*GAMMA RAY BURSTS/*GAMMA RAY OBSERVATORY/*RADIATION
      SOURCES
MINS: / BALLOON-BORNE INSTRUMENTS/ SPECTRUM ANALYSIS/ X RAY SPECTRA
ABA: Author
ABS: Miscellaneous tasks related to the development of the Bursts and Transient
      Source Experiment on the Gamma Ray Observatory and to analysis of archival
      data from balloon flight experiments were performed. The results are
      summarized and relevant references are included.

ENTER: